Ca(OH)(2) coated nanoscale zero-valent iron as a persulfate activator for the degradation of sulfamethazine in aqueous solution

Junmin Deng, Haoran Dong, Long Li, Yaoyao Wang, Qin Ning, Bin Wang, Guangming Zeng

$Ca(OH)_2$ coated nanoscale zero-valent iron as a persulfate activator for the degradation of sulfamethazine in aqueous solution

Junmin Deng[1,2,3], Haoran Dong[1,2,*], Long Li[1,2], Yaoyao Wang[1,2], Qin Ning[1,2], Bin Wang[1,2], Guangming Zeng[1,2]

1. College of Environmental Science and Engineering, Hunan University, Changsha, Hunan 410082, China.
2. Key Laboratory of Environmental Biology and Pollution Control (Hunan University), Ministry of Education, Changsha, Hunan 410082, China
3. University of Rennes, Ecole Nationale Supérieure de Chimie de Rennes, CNRS, ISCR-UMR6226, F-35000 Rennes, France

*Corresponding author. E-mail: dongh@hnu.edu.cn; Tel: (+86)-0731-88822778

Abstract

In this work, a novel composite, $Ca(OH)_2$ coated nanoscale zero-valent iron (denoted as nZVI-$Ca(OH)_2$), was synthesized and used as an activator of persulfate for the degradation of sulfamethazine (SMT). The effects of sonication time during composite synthesis, pH, nZVI-$Ca(OH)_2$ dosage and typical groundwater components were investigated by batch experiments. Sonication time during the synthesis of the composite could affect the thickness of $Ca(OH)_2$ shell, however, it exerted no obvious

effect on SMT removal by nZVI-$Ca(OH)_2$ activated persulfate. The initial pH also had insignificant effect on SMT removal in nZVI-$Ca(OH)_2$/persulfate system. There was an optimum dosage of nZVI-$Ca(OH)_2$ composites for the activation of persulfate, and the SMT removal efficiency decreased at both higher and lower dosage. The efficient performance of nZVI-$Ca(OH)_2$ in synthetic groundwater was observed over a wide pH range (3-9). However, with the presence of high concentration of HCO_3^- or SO_4^{2-}, SMT removal was inhibited greatly due to the quenching of radicals by HCO_3^- or SO_4^{2-} and the buffering effect of HCO_3^-. In addition, the longevity of nZVI-$Ca(OH)_2$ was also investigated. Even after 30 days of aging in the air, Fe^0 could still be detected in nZVI-$Ca(OH)_2$. Despite some loss of Fe^0, the composites kept high reactivity for activation of persulfate for SMT removal, which might be attributed to the excellent activation ability of amorphous iron oxides. To sum up, the $Ca(OH)_2$-shell can protect the inner iron core and consequently prolong the lifetime of nZVI.

Keywords

Calcium hydroxide; Surface coating; Nanoscale zero-valent iron; Persulfate; Sulfamethazine

Introduction

In recent decades, nanoscale zero-valent iron (nZVI) has been widely applied in water treatment and soil/groundwater remediation processes [1]. Due to its high

reactivity, nZVI has been applied to remove various environmental contaminants, such as chlorinated organic compounds and heavy metals [2-4]. Apart from directly using nZVI to reduce pollutant, nZVI can also perform heterogeneous catalysis in advanced oxidation system which is more effective for the treatment of refractory organic pollutants [5, 6]. Recently, nZVI has been reported to be an efficient activator of persulfate for the treatment of various organic contaminants [7-9].

Since nZVI particles have large specific surface area and high reactivity [10], Fe^0 can easily release Fe^{2+} in the presence of dissolved oxygen and persulfate (Eq. 1-2). And then those ferrous ions activate $S_2O_8^{2-}$ to produce sulfate radicals and hydroxyl radicals which can react with various environmental pollutants (Eq. 3 and 4). Furthermore, Fe^{3+} generated from these reactions reacts with Fe^0 sequentially to give a sustained supply of Fe^{2+} (Eq. 5) [11].

$$2Fe^0 + O_2 + 2H_2O \rightarrow 2Fe^{2+} + 4OH^- \quad (1)$$

$$Fe^0 + S_2O_8^{2-} \rightarrow Fe^{2+} + 2SO_4^{2-} \quad (2)$$

$$S_2O_8^{2-} + Fe^{2+} \rightarrow Fe^{3+} + SO_4^{2-} + SO_4^{\cdot -} \quad (3)$$

$$SO_4^{\cdot -} + H_2O \rightarrow \cdot OH + SO_4^{2-} + H^+ \quad (4)$$

$$2Fe^{3+} + Fe^0 \rightarrow 3Fe^{2+} \quad (5)$$

However, strong magnetic attraction and van der waals force between nZVI nanoparticles cause them to aggregate into larger size particles [12-18]. The increased size of these cluster result in a sharp decrease in surface area and poor dispersion of nZVI in aqueous solution [13,14]. Thus, to overcome the aggregation of nZVI,

researchers have attempted different stabilization methods for its effective environmental application [12,19,20]. Some supporting materials (e.g., clay, zeolite and biochar) and surface stabilizers (e.g., surfactant, synthetic or natural macromolecule or polyelectrolyte) were chosen to stabilize nZVI [12]. However, the issues concerning the effective release of reactive iron from the supporting material and the reactivity loss after surface modification by surface stabilizer adsorption were reported [15,21,22]. Besides the above supporters and organic stabilizers, one kind of releasable inorganic shell ($Ca(OH)_2$) on nZVI surface was developed [23]. It was reported that the $Ca(OH)_2$ coating layer can effectively enhance the stability and mobility of nZVI. Depending on the solubility of $Ca(OH)_2$, the $Ca(OH)_2$ coating on nZVI surface was supposed as a releasable shell during application for onsite remediation, thus, it would not result in a reactivity loss of nZVI.

Given that one drawback in nZVI+persulfate system is that the activation reactions usually proceed rapidly, resulting in self-quenching of radicals [24], it was presumed that the moderately soluble $Ca(OH)_2$ layer might control the persulfate activation rate by nZVI. Up to date, no studies have applied the $Ca(OH)_2$ coated nZVI (nZVI-$Ca(OH)_2$) for persulfate activation. In this study, nZVI-$Ca(OH)_2$ composites were synthesized for the activation of persulfate. Sulfamethazine (SMT) was chosen as a model contaminant, not only because it is one of frequently detected pharmaceutical compounds in aqueous environment, but the mechanism of SMT degradation by sulfate radicals has been well established in many studies [25,26]. The

effects of critical factors such as coating thickness, initial pH, nZVI-$Ca(OH)_2$ dosage and typical groundwater components were examined. Furthermore, aging experiments were carried out to study the transformation of nZVI-$Ca(OH)_2$ in air and its reactivity evolution with aging time.

2. Materials and methods

2.1. Chemicals

All chemicals used in this study were of analytical grade and used as received without further purification. Sulfamethazine (SMT, ≥99%, w/w) was obtained from Sigma Chemical Company (Beijing, China). HCl, NaOH, $CaCl_2$, $FeCl_3 \cdot 6H_2O$, NaCl, $NaHCO_3$, $NaSO_4$, $NaBH_4$, $Na_2S_2O_8$, ethanol and n-butanol were all purchased form Damao Chemical Reagent Factory(Tianjin, China). Synthetic groundwater was prepared according to our previous work [27], containing Na^+ (230 mg/L), Ca^{2+} (32 mg/L), HCO_3^- (183 mg/L), SO_4^{2-} (96 mg/L) and Cl^- (234 mg/L).

2.2. Preparation of $Ca(OH)_2$ coated nZVI composites

nZVI was prepared following the liquid phase reduction method as described in our previous study [15, 28]. In brief, with N_2 purging, 100 mL $NaBH_4$ solution (0.2 M) was added dropwise into 100 mL of a 0.05 M $FeCl_3$ solution with strong mechanical stirring. After that, the suspension was stirred for another 30 min. Then the synthesized nZVI particles were separated by a magnet, and washed three times

with ethanol. After vacuum dried at 60°C for 8 h, the nZVI particles were collected and stored in sealing bags at 4°C in order to avoid oxidization before further modification.

A surface precipitation method was employed to prepare $Ca(OH)_2$ coated nZVI composites [23]. Firstly, $CaCl_2$ (0.025 M) and NaOH (0.05 M) solutions were prepared with ethanol. Then, 600 mg nZVI particles were added into 200 mL NaOH solution. After mixing in a sonication bath for 5 min, the $CaCl_2$ solution was quickly introduced into the nZVI suspension. After that, the mixture was placed in a sonication bath at 60 ℃ during the coating process. Then the $Ca(OH)_2$ coated nZVI particles were magnetically separated from $Ca(OH)_2$ particles. These separated particles were thoroughly washed with ethanol and vacuum dried. The synthesized nZVI- $Ca(OH)_2$ particles were stored at 4°C before use.

2.3. Batch experiments

2.3.1. SMT-removal experiments

The SMT removal experiments were conducted in 250 mL glass bottles in the dark. In a typical run, 250 mL SMT (0.1 mM) and 100 mL persulfate solutions were introduced in 650 mL water to achieve a SMT concentration of 0.025 mM and persulfate concentration of 1 mM. The reason for the use of higher concentration of SMT (~ 6.9 mg/L) than the realistic concentration (~μg/L) in natural waters was to facilitate the detection of SMT loss and examine the removal capacity of the oxidation

process. After adjusting the solution pH, the mixture was transferred to bottles (with 200 mL for each). Finally, nZVI-$Ca(OH)_2$ particles (10 mg) were added into the bottles, and immediately transferred to a vapour bathing constant temperature vibrator at 20.0 ± 0.2 °C for reaction up to 1 h. At predetermined time intervals, 1 mL of samples were extracted from the suspension and filtered through 0.22-μm membranes, and immediately quenched with 20 μL n-butanol (controlled experiments of SMT removal quenched with n-butanol are shown in Fig. S1). During the reaction period, the pH was monitored by using a pH meter (INESA, PHS-3C).

The concentration of SMT was measured using an Agilent 1200 high performance liquid chromatography (HPLC) with a C18 reversed-phase column (4.6 mm×150 mm). The mobile phase was acetonitrile and ultrapure water (35:65, v/v) with a flow rate of 1.0 mL/min. The temperature of column was 25 °C, and the sample injection volume was 20 μL. UV detection at a wavelength of 266 nm was used to quantify SMT [25]. The SMT removal efficiency (η, 100%) was calculated with the following equation:

$$\eta = \frac{C_0 - C_r}{C_0} \times 100\% \quad (6)$$

where C_0 (mg/L) is the initial concentration of SMT, Cr (mg/L) is the residue SMT concentration.

Unless stated otherwise, all experiments in this study were performed in triplicate. The reported data took the mean values of each experimental value, and the error bars were presented as well.

2.3.2. Aging experiments

Aging of nZVI-$Ca(OH)_2$ particles was carried out in the air at room temperature. At certain intervals (5 d, 10 d, 20 d and 30 d), 100 mg of aged samples were collected, characterized and applied for the successive SMT removal experiments under the same condition as described above.

2.4. Characterization and analysis

The morphological images of nZVI-$Ca(OH)_2$ particles were recorded with a scanning electron microscope (SEM, JSM-6700). Energy dispersive X-ray spectroscopy (EDS) was coupled with SEM to examine the element on the particle surface. The mass ratio of $Ca(OH)_2$ in the composite of nZVI-$Ca(OH)_2$ was measured by analyzing the Fe and Ca concentration in acid-digestion solution of nZVI-$Ca(OH)_2$ with Atomic Absorption Spectrophotometer (AAS, PEAA700). The crystalline phases were identified with an X-ray diffractometer (XRD, Philips Electronic Instruments).

3. Results and discussions

3.1. Characterization of nZVI-$Ca(OH)_2$ composites

The SEM image of nZVI-$Ca(OH)_2$ composite is presented in Fig. 1a. nZVI-$Ca(OH)_2$ particles are in the size range of nanoscale with shape of sphere. These particles existed in the form of chain-like aggregates. It is noticeable that these nanoparticles were covered by a thin coating layer of several nanometer thickness,

161 which might be the $Ca(OH)_2$ shell. Further EDS elemental analysis of nZVI-$Ca(OH)_2$
162 shows a strong Fe peak and a weak Ca peak, indicating the existence of Ca on the
163 surface of composite (Fig. 1b).

164 The chemical components of nZVI-$Ca(OH)_2$ were characterized by the XRD
165 (Fig. 1c). As observed, there is a strong peak at 44.5° which should be assigned to Fe
166 (0) [29, 30], while no obvious peaks of $Ca(OH)_2$ were found. Similar phenomena
167 were also reported in other studies [23, 31], in which XRD was used to characterize
168 surface coated nZVI with $Ca(OH)_2$ and $Al(OH)_3$, and it was found that neither
169 $Ca(OH)_2$ nor $Al(OH)_3$ was observed. This might be due to their low concentrations or
170 low degree of crystallinity.

171 In order to figure out the $Ca(OH)_2$ content coated on nZVI, AAS was used to
172 determine the ratio of Fe and Ca after acid digestion of the nZVI-$Ca(OH)_2$
173 composites. Fig. 1d shows the content of $Ca(OH)_2$ coated on the nZVI particles under
174 different sonication time. It is clear that the sonication time did significantly affect the
175 coating thickness. The amount of $Ca(OH)_2$ was 1.31% of the total weight after 0.5 h
176 coating, which rose to 10.19% after 4 h coating. To verify the effect of $Ca(OH)_2$
177 coating on the mobility of nZVI particles, a simplified sand column test was carried
178 out and the results show that the $Ca(OH)_2$ coating did improve the transport of nZVI
179 particles in porous media (Fig. S2). This is consistent with the finding in literature
180 [23]. However, no obvious difference was observed for the nZVI-$Ca(OH)_2$ with
181 different amount of $Ca(OH)_2$ (data not shown). In view of the effect of sonication time

182 on coating thickness, it may influence the reactivity of the composite, which will be
183 discussed in the following part. Overall, the results from SEM, EDS, XRD, AAS
184 analysis and mobility test, collectively, suggested the successful synthesis of nZVI-
185 $Ca(OH)_2$ composite.

186 **3.2. Removal of SMT in nZVI-$Ca(OH)_2$/persulfate system**

187 **3.2.1. Effect of sonication time**

188 As mentioned above, the sonication time during synthesis can affect the
189 percentage of $Ca(OH)_2$ on nZVI-$Ca(OH)_2$ particle surface. It could possibly be a
190 critical factor in SMT removal by nZVI-$Ca(OH)_2$ activated persulfate. Thus, effect of
191 sonication time on SMT removal was investigated (Fig. 2). As observed, both removal
192 efficiency and reaction rates of SMT were almost overlapped at different conditions.
193 With the sonication time varied from 0.5 h to 4 h, SMT removal efficiency could
194 reach about 100% after 1 h reaction time. Even though the sonication time affected
195 the $Ca(OH)_2$ coating thickness on nZVI surface, it seems had little influence on SMT
196 removal in persulfate system. Since 0.5 h sonication time was long enough to give an
197 excellent performance in SMT removal for nZVI-$Ca(OH)_2$, it was selected for the
198 preparation of nZVI-$Ca(OH)_2$ in the following study.

199 **3.2.2. Effect of initial pH**

200 SMT removal experiments were carried out at four different initial pH values, i.e. 3, 5,
201 7 and 9. As shown in Fig. 3a, the final removal efficiency as well as the removal

kinetics were much similar at initial pH from 3 to 9. In order to probe into the underlying mechanism, the changes of pH during reaction were monitored (Fig. 3b). Obviously, no matter at what initial pH value, the solution pH dropped dramatically (within 10 min) to around 3.5 and finally maintained in a very narrow pH range of 3.0 to 3.2. This should be the reason for the similar SMT removal under various pH conditions. The sharp pH change may be due to the release of H^+ from the reaction of Fe^{3+} precipitation (Eq. 7) [11], the reaction between $SO_4^{\cdot-}$ and H_2O (Eq. 4) or the reaction of Fe^0 with persulfate (Eq. 8) [32]. Although the dissolution of the outside $Ca(OH)_2$ layer would consume protons and then cause a rise in solution pH (Eq. 9), the mass ratio of $Ca(OH)_2$ is extremely low (1.31%), the influence of $Ca(OH)_2$ layer on solution pH should be negligible.

$$Fe^{3+} + 3H_2O \rightarrow Fe(OH)_3(s) + 3H^+ \quad (7)$$

$$Fe^0 + S_2O_8^{2-} + 2H_2O \rightarrow Fe^{2+} + 2 \bullet OH + 2SO_4^{2-} + 2H^+ \quad (8)$$

$$Ca(OH)_2 + 2H^+ \rightarrow Ca^{2+} + 2H_2O \quad (9)$$

3.2.3. Effect of nZVI-$Ca(OH)_2$ dosage

The effect of nZVI-$Ca(OH)_2$ dosage on SMT removal was investigated over a range of 10–200 mg/L and the results are illustrated in Fig. 4a. The removal efficiency was 90.31%, 100%, 93.14% and 77.03% with the composite dosage of 10, 50, 100 and 200 mg/L, respectively. With the increasing nZVI-$Ca(OH)_2$ dosage from 10 to 50 mg/L, SMT removal efficiency was improved. This should be due to the generation of

223 more amounts of radicals with the existence of more iron ions in the solution. When
224 the dose was further increased up to 200 mg/L, the removal efficiency dropped
225 significantly to 77.03%. To find out the difference among the reaction systems with
226 varying nZVI-Ca(OH)$_2$ dosage, the pH changes with time in different systems were
227 measured (Fig. 4b). The pH changes in systems of 10 and 50 mg/L showed a similar
228 trend, i.e., a drastic drop in the first 5 min followed by a gradual slowdown. While the
229 systems of 100 and 200 mg/L displayed a very different way with pH increase after
230 the sharp decrease in the first 5 min. As discussed earlier, this sharp pH decrease was
231 mainly attributed to the release of H^+ during the reactions. While for the system of
232 100 and 200 mg/L, the following pH rise may be due to the dissolution of excessive
233 nZVI-Ca(OH)$_2$ (Eq. 9 and Eq. 10). The rapid consumption of H^+ and release of OH^-
234 could lead to an increase in solution pH.

235 $$Fe^0 + 2H_2O \rightarrow Fe^{2+} + H_2 + 2OH^- \quad (10)$$

236 With the increase of nZVI-Ca(OH)$_2$ dosage form 50 mg/L to 200 mg/L, the
237 dissolution of excessive catalyst would cause a rise of solution pH as well as a break
238 out of ferrous ions. These ferrous ions could possibly have a scavenging effect on
239 radicals (Eq. 11), and thus lowering the removal efficiency of SMT [33]. Moreover,
240 the existence of dissolved iron could be just temporarily, under such pH condition,
241 they could easily tend to get hydrolysis [34]. According to Eq. 3, 11 and 12, the lack
242 of Fe^{2+}/Fe^{3+} would inhibit the formation of sulfate radicals, and then further resulted
243 in a relative low removal efficiency of SMT [35].

244 $$Fe^{2+} + SO_4^{\cdot-} \rightarrow Fe^{3+} + SO_4^{2-} \quad (11)$$

245 $$Fe^{3+} + S_2O_8^{2-} \rightarrow Fe^{2+} + S_2O_8^{\cdot-} \quad (12)$$

246 **3.2.4. Effect of typical groundwater components**

247 In natural groundwater, there are many kinds of components that may have some
248 effects on the contaminant removal process. In this study, experiments were carried
249 out in synthetic groundwater under different pH conditions. As demonstrated in Fig.
250 5a, SMT was removed efficiently at all pH values. However, the reaction rate at pH 9
251 was much slower than that at other pH values. Specifically, the removal efficiency of
252 SMT at pH 9 was just approximately 15.19% after reaction for 5 min, while around
253 48.92%, 57.18% and 52.62% were obtained at pH 3, pH 5 and pH 7, respectively. The
254 evolution of pH at different initial pH values was monitored (Fig. 5b). Different from
255 the rapid pH drop in pure water condition, much less changes of pH were observed
256 during the reaction in synthetic groundwater. This should be result from the good
257 buffer capacity of HCO_3^-. Under alkaline condition, nZVI-$Ca(OH)_2$ could hardly be
258 dissolved and also it would be favorable for the precipitation of Fe^{2+}/Fe^{3+}, thus, there
259 would be less free iron ions existed in the system, resulting in the less activation of
260 persulfate [36]. Pang et al. [36] reported that ultrasound irradiation could contribute to
261 acceleration of ZVI corrosion and removal of passive films, resulting in high
262 efficiency in peroxymonosulfate activation. Thus, the precipitation of Fe^{2+}/Fe^{3+} could
263 possibly be one reason for the slower removal rate of SMT at pH 9. Besides,
264 bicarbonate can be a scavenger of sulfate radicals (Eq. 13). Although other radicals

(i.e. $CO_3^{\cdot-}$) are generated from the scavenging reaction, they are quite unreactive compared to $SO_4^{\cdot-}$ toward most organic substrates in aqueous condition [37].

$$SO_4^{\cdot-} + HCO_3^- \rightarrow H^+ + SO_4^{2-} + CO_3^{\cdot-} \quad (13)$$

In addition, previous studies reported that SO_4^{2-} could also exhibit negative effect on the radical-based reactions [38]. SO_4^{2-} ions can form bonding with Fe^{2+} and Fe^{3+}, producing complexes of $FeSO_4$ and $Fe_2(SO_4)_3$. These complex reactions reduced the concentration of free iron ions in the solution for activation of persulfate, thus inhibiting the removal of SMT.

To further identify the role of each individual component, SMT removal in the presence of single ions (i.e., HCO_3^-, SO_4^{2-}, Cl^- and Ca^{2+}) was examined respectively with different concentration. As shown in Fig. 6a, all these ions with a lower concentration (1 mmol/L) could barely affect the nZVI-$Ca(OH)_2$ performance on SMT removal. Only in the case of HCO_3^-, a slower removal rate was observed. However, after 60 min reaction time, the removal efficiency reached 100% in all reaction systems. When increasing the concentration to 10 mmol/L, the groundwater components showed very different impacts on the removal performance (Fig. 6b). Ca^{2+} and Cl^- had insignificant impact on SMT removal, while the presence of HCO_3^- or SO_4^{2-} substantially decreased the SMT removal. The results verified the previous assumption that the drop of SMT removal efficiency in synthetic groundwater was mainly due to the effect of HCO_3^- and SO_4^{2-}.

To sum up, the effect of these typical groundwater components at low

concentration were negligible, and even at higher concentration Cl^- and Ca^{2+} had little effect on SMT removal. While HCO_3^- or SO_4^{2-} with higher concentration could inhibit the degradation efficiency of SMT and the inhibiting effect of HCO_3^- was more pronounced than the other ions at the same concentration.

3.2.5 Effect of particle aging

To further verify whether the $Ca(OH)_2$ coating could alleviate the surface passivation of nZVI caused by corrosion, the nZVI-$Ca(OH)_2$ particles were aged in the open air for different time. Then, the removal of SMT by the aged nZVI-$Ca(OH)_2$ activated PS were tested for comparison (Fig. 7a). The results show that, after aging up to 30 days, nZVI-$Ca(OH)_2$ still kept a high capacity of PS activation for the SMT degradation.

The reactivity of nZVI-$Ca(OH)_2$ was associated with its surface composition, XRD analysis was then conducted to identify the composition evolution and crystalline change of nZVI-$Ca(OH)_2$ with aging time. Fig. 7b shows the XRD patterns of fresh and different aged nZVI-$Ca(OH)_2$. It is noticeable that the peak of Fe^0 at 44.5° became weaker with aging time. But the Fe^0 peak can still be detected even after 30 days of aging, indicating the existence of Fe^0 on the surface of particles after 30 days. Our previous study on Fe/Ni bimetal nanoparticles aging process reported that the Fe^0 peak disappeared in just 5 days [29]. In comparison, it was clear that coating nZVI with $Ca(OH)_2$ did prolong its lifetime due to the protection of $Ca(OH)_2$

306 outer shell. For the aged samples, peaks assigned to iron oxide were not detected,
307 which is quite different from the reported XRD patterns of aged nZVI. Typical aging
308 products of nZVI in oxic condition are goethite, maghemite, magnetite and
309 lepidocrocite [39]. Whilst, there were no iron oxides detected in the aging samples of
310 nZVI-$Ca(OH)_2$, which manifests that the corrosion of nZVI in nZVI-$Ca(OH)_2$ was not
311 significant and iron oxides were not existing in crystalline phrase.

312 Even though there were some loss of Fe^0 with aging, SMT removal efficiency
313 was barely influenced. This could possibly be attributed to the good persulfate
314 activation capacity of amorphous iron oxides [40]. Since both Fe^0 and iron oxides can
315 activate persulfate, fresh and aged nZVI-$Ca(OH)_2$ samples showed similar
316 performance in the process of SMT degradation.

317 **4. Conclusion**

318 In this study, a thin $Ca(OH)_2$ shell was successfully coated on the surface of
319 nZVI particles. The thickness of $Ca(OH)_2$ is related to sonication time during
320 synthesis, the longer sonication time the more $Ca(OH)_2$ coated. Then, nZVI-$Ca(OH)_2$
321 composites were utilized as an activator of persulfate to remove SMT. The effects of
322 sonication time, pH, nZVI-$Ca(OH)_2$ dosage and typical groundwater components
323 were investigated. The following conclusions were made:

324 - The sonication time and initial pH had little effect on SMT removal by
325 nZVI-$Ca(OH)_2$/persulfate system, while nZVI-$Ca(OH)_2$ dosage affected the

removal efficiency of SMT greatly. There was an optimum dosage of nZVI-$Ca(OH)_2$, at higher or lower dosage, the SMT removal was decreased.

- nZVI-$Ca(OH)_2$ showed different performance in synthetic groundwater and pure water over the pH range of 3-9. The effect of typical groundwater components (Ca^{2+}, Cl^-, HCO_3^- and SO_4^{2-}) were examined respectively and it was found that the groundwater ions at low concentration showed negligible influence on SMT removal, but HCO_3^- and SO_4^{2-} at high concentration could inhibit the SMT removal in a large degree.
- Effect of aging time on the reactivity of nZVI-$Ca(OH)_2$ was investigated, and it was found that the particles kept its reactivity even after 30 days of aging. This suggests that coating nZVI with $Ca(OH)_2$ did prolong the lifetime of nZVI.

Acknowledgments

This research was supported by the National Natural Science Foundation of China (51879100) and the Program for Changjiang Scholars and Innovative Research Team in University (IRT-13R17).

References

[1] X. Guan, Y. Sun, H. Qin, J. Li, I.M. Lo, D. He, H. Dong, The limitations of applying zero-valent iron technology in contaminants sequestration and the corresponding countermeasures: the development in zero-valent iron technology in

347 the last two decades (1994-2014), Water research, 75 (2015) 224-248.

348 [2] T. Phenrat, I. Kumloet, Electromagnetic induction of nanoscale zerovalent iron
349 particles accelerates the degradation of chlorinated dense non-aqueous phase liquid:
350 Proof of concept, Water research, 107 (2016) 19-28.

351 [3] H.R. Dong, L. Li, Y. Lu, Y. Cheng, Y. Wang, Q. Ning, B. Wang, L. Zhang, G.
352 Zeng., Integration of nanoscale zero-valent iron and functional anaerobic bacteria for
353 groundwater remediation: A review. Environment International. 124 (2019) 265-277.

354 [4] Y.J. Cheng, H. Dong, Y. Lu, K. Hou, Y. Wang, Q. Ning, L. Li, B. Wang, L.
355 Zhang, G. Zeng. Toxicity of sulfide-modified nanoscale zero-valent iron to
356 Escherichia coli in aqueous solutions. Chemosphere, 220 (2019) 523-530.

357 [5] Kong, L.J., Zhu, Y., Liu, M., Chang, X., Xiong, Y., Chen, D., Conversion of Fe-
358 rich waste sludge into nano-flake Fe-SC hybrid Fenton-like catalyst for degradation of
359 AOII, Environmental Pollution. 216 (2016) 568-574.

360 [6] I. Mikhailov, S. Komarov, V. Levina, A. Gusev, J.P. Issi, D. Kuznetsov,
361 Nanosized zero-valent iron as Fenton-like reagent for ultrasonic-assisted leaching of
362 zinc from blast furnace sludge, Journal of hazardous materials, 321 (2017) 557-565.

363 [7] H. Dong, Q. He, G. Zeng, L. Tang, L. Zhang, Y. Xie, Y. Zeng, F. Zhao,
364 Degradation of trichloroethene by nanoscale zero-valent iron (nZVI) and nZVI
365 activated persulfate in the absence and presence of EDTA, Chemical Engineering
366 Journal, 316 (2017) 410-418.

367 [8] N. Barhoumi, N. Oturan, H. Olvera-Vargas, E. Brillas, A. Gadri, S. Ammar, M.A.

368 Oturan, Pyrite as a sustainable catalyst in electro-Fenton process for improving
369 oxidation of sulfamethazine. Kinetics, mechanism and toxicity assessment, Water
370 research, 94 (2016) 52-61.
371 [9] J. Yan, H. Lu, W. Gao, X. Song, M. Chen, Biochar supported nanoscale
372 zerovalent iron composite used as persulfate activator for removing trichloroethylene,
373 Bioresource technology, 175 (2015) 269-274.
374 [10] H.R. Dong, Y. Cheng, Y. Lu, K. Hou, L. Zhang, L. Li, B. Wang, Y. Wang,Q.
375 Ning, G. Zeng. Comparison of toxicity of Fe/Ni and starch-stabilized Fe/Ni
376 nanoparticles toward Escherichia coli. Separation and Purification Technology, 210
377 (2019) 504–510.
378 [11] C. Kim, J.Y. Ahn, T.Y. Kim, W.S. Shin, I. Hwang, Activation of Persulfate by
379 Nanosized Zero-valent Iron (NZVI): Mechanisms and Transformation Products of
380 NZVI, Environmental science & technology, 52 (2018) 3625-3633.
381 [12] H. Dong, Y. Xie, G. Zeng, L. Tang, J. Liang, Q. He, F. Zhao, Y. Zeng, Y. Wu,
382 The dual effects of carboxymethyl cellulose on the colloidal stability and toxicity of
383 nanoscale zero-valent iron, Chemosphere, 144 (2016) 1682-1689.
384 [13] P. Tanapon, S. Navid, S. Kevin, R.D. Tilton, G.V. Lowry, Aggregation and
385 sedimentation of aqueous nanoscale zerovalent iron dispersions, Environmental
386 science & technology, 41 (2007) 284-290.
387 [14] X.Q. Li, D.W. Elliott, W.X. Zhang, Zero-Valent Iron Nanoparticles for
388 Abatement of Environmental Pollutants: Materials and Engineering Aspects, Critical

389 Reviews in Solid State & Materials Sciences, 31 (2006) 111-122.

390 [15] H. Dong, J. Deng, Y. Xie, C. Zhang, Z. Jiang, Y. Cheng, K. Hou, G. Zeng,
391 Stabilization of nanoscale zero-valent iron (nZVI) with modified biochar for Cr(VI)
392 removal from aqueous solution, Journal of hazardous materials, 332 (2017) 79-86.

393 [16] Y. Zhang, Y. Li, J. Li, G. Sheng, Z. Yun, X. Zheng, Enhanced Cr(VI) removal by
394 using the mixture of pillared bentonite and zero-valent iron, Chemical Engineering
395 Journal, 185-186 (2012) 243-249.

396 [17] L. Changha, D.L. Sedlak, Enhanced formation of oxidants from bimetallic
397 nickel-iron nanoparticles in the presence of oxygen, Environmental science &
398 technology, 42 (2008) 8528-8533.

399 [18] H.L. Lien, W.X. Zhang, Nanoscale Pd/Fe bimetallic particles: Catalytic effects of
400 palladium on hydrodechlorination, Applied Catalysis B Environmental, 77 (2007)
401 110-116.

402 [19] H. Dong, C. Zhang, K. Hou, Y. Cheng, J. Deng, Z. Jiang, L. Tang, G. Zeng,
403 Removal of trichloroethylene by biochar supported nanoscale zero-valent iron in
404 aqueous solution, Separation and Purification Technology, 188 (2017) 188-196.

405 [20] O.S. Arvaniti, Reductive Degradation of Perfluorinated Compounds in Water
406 using Mg- aminoclay coated Nanoscale Zero Valent Iron, Chemical Engineering
407 Journal, 262 (2015) 133-139.

408 [21] H.R. Dong, Q. He, G.M. Zeng, L. Tang, C. Zhang, Y.K. Xie, Y.L. Zeng, F. Zhao,
409 Y. Wu. Chromate removal by surface-modified nanoscale zero-valent iron: Effect of

410 different surface coatings and water chemistry, Journal of Colloid and Interface
411 Science, 471 (2016) 7-13.
412 [22] Dong, HR; Hou, KJ; Qiao, WW; Cheng, YJ; Zhang, LH; Wang, B; Li, L; Wang,
413 YY; Ning, Q; Zeng, GM. Insights into enhanced removal of TCE utilizing sulfide-
414 modified nanoscale zero-valent iron activated persulfate, Chemical Engineering
415 Journal, 359 (2019) 1046-1055.
416 [23] W. Cai-Jie, L. Xiao-Yan, Surface coating with Ca(OH)2 for improvement of the
417 transport of nanoscale zero-valent iron (nZVI) in porous media, Water Science &
418 Technology A Journal of the International Association on Water Pollution Research,
419 68 (2013) 2287.
420 [24] Y.G. Kang, H. Yoon, W. Lee, E.J. Kim, Y.S. Chang, Comparative study of
421 peroxide oxidants activated by nZVI: Removal of 1,4-Dioxane and arsenic(III) in
422 contaminated waters, Chemical Engineering Journal, 334 (2018) 2511-2519.
423 [25] Y.-q. Gao, N.-y. Gao, Y. Deng, Y.-q. Yang, Y. Ma, Ultraviolet (UV) light-
424 activated persulfate oxidation of sulfamethazine in water, Chemical Engineering
425 Journal, 195-196 (2012) 248-253.
426 [26] Y. Fan, Y. Ji, D. Kong, J. Lu, Q. Zhou, Kinetic and mechanistic investigations of
427 the degradation of sulfamethazine in heat-activated persulfate oxidation process,
428 Journal of hazardous materials, 300 (2015) 39-47.
429 [27] Y. Xie, H. Dong, G. Zeng, L. Zhang, Y. Cheng, K. Hou, Z. Jiang, C. Zhang, J.
430 Deng, The comparison of Se(IV) and Se(VI) sequestration by nanoscale zero-valent

431 iron in aqueous solutions: The roles of solution chemistry, Journal of hazardous
432 materials, 338 (2017) 306-312.
433 [28] J. Deng, H. Dong, C. Zhang, Z. Jiang, Y. Cheng, K. Hou, L. Zhang, C. Fan,
434 Nanoscale zero-valent iron/biochar composite as an activator for Fenton-like removal
435 of sulfamethazine, Separation and Purification Technology, 202 (2018) 130-137.
436 [29] H. Dong, Z. Jiang, J. Deng, C. Zhang, Y. Cheng, K. Hou, L. Zhang, L. Tang, G.
437 Zeng, Physicochemical transformation of Fe/Ni bimetallic nanoparticles during aging
438 in simulated groundwater and the consequent effect on contaminant removal, Water
439 research, 129 (2017) 51-57.
440 [30] H. Dong, C. Zhang, J. Deng, Z. Jiang, L. Zhang, Y. Cheng, K. Hou, L. Tang, G.
441 Zeng, Factors influencing degradation of trichloroethylene by sulfide-modified
442 nanoscale zero-valent iron in aqueous solution, Water research, 135 (2018) 1-10.
443 [31] Y.B. Hu, X.Y. Li, Influence of a thin aluminum hydroxide coating layer on the
444 suspension stability and reductive reactivity of nanoscale zero-valent iron, Applied
445 Catalysis B Environmental, 226 (2018) 554-564.
446 [32] H. Li, J. Wan, Y. Ma, Y. Wang, M. Huang, Influence of particle size of zero-
447 valent iron and dissolved silica on the reactivity of activated persulfate for
448 degradation of acid orange 7, Chemical Engineering Journal, 237 (2014) 487-496.
449 [33] J. Deng, Y. Shao, N. Gao, Y. Deng, C. Tan, S. Zhou, Zero-valent
450 iron/persulfate(Fe 0 /PS) oxidation acetaminophen in water, International Journal of
451 Environmental Science & Technology, 11 (2014) 881-890.

452 [34] H.J. Fan, S.T. Huang, W.H. Chung, J.L. Jan, W.Y. Lin, C.C. Chen, Degradation
453 pathways of crystal violet by Fenton and Fenton-like systems: Condition optimization
454 and intermediate separation and identification, Journal of hazardous materials, 171
455 (2009) 1032-1044.
456 [35] O. Seok-Young, K. Hyeong-Woo, P. Jun-Mo, P. Hung-Suck, Y. Chohee,
457 Oxidation of polyvinyl alcohol by persulfate activated with heat, Fe2+, and zero-
458 valent iron, Journal of hazardous materials, 168 (2009) 346-351.
459 [36] Pang, Y.X., Ruan, Y., Feng, Y., Diao, Z., Shih, K. Hou, L., Chen, D., Kong, L.J.,
460 Ultrasound assisted zero valent iron corrosion for peroxymonosulfate activation for
461 Rhodamine-B degradation, Chemosphere, 228 (2019) 412-417.
462 [37] L.W. Matzek, K.E. Carter, Sustained persulfate activation using solid iron:
463 kinetics and application to ciprofloxacin degradation, Chemical Engineering Journal,
464 307 (2017) 650-660.
465 [38] H. Dong, B. Wang, L. Li, Y. Wang, Q. Ning, R. Tian, R. Li, J. Chen, Q. Xie.
466 Activation of persulfate and hydrogen peroxide by using sulfide-modified nanoscale
467 zero-valent iron for oxidative degradation of sulfamethazine: A comparative study.
468 Separation and Purification Technology, 218 (2019) 113-119.
469 [39] S. Bae, R.N. Collins, T.D. Waite, K. Hanna, Advances in surface passivation of
470 nanoscale zerovalent iron (NZVI): A critical review, Environmental science &
471 technology, 52 (2018) 12010–12025.
472 [40] Y.H. Jo, S.H. Do, S.H. Kong, Persulfate activation by iron oxide-immobilized

473 MnO_2 composite: Identification of iron oxide and the optimum pH for degradations,

474 Chemosphere, 95 (2014) 550-555.

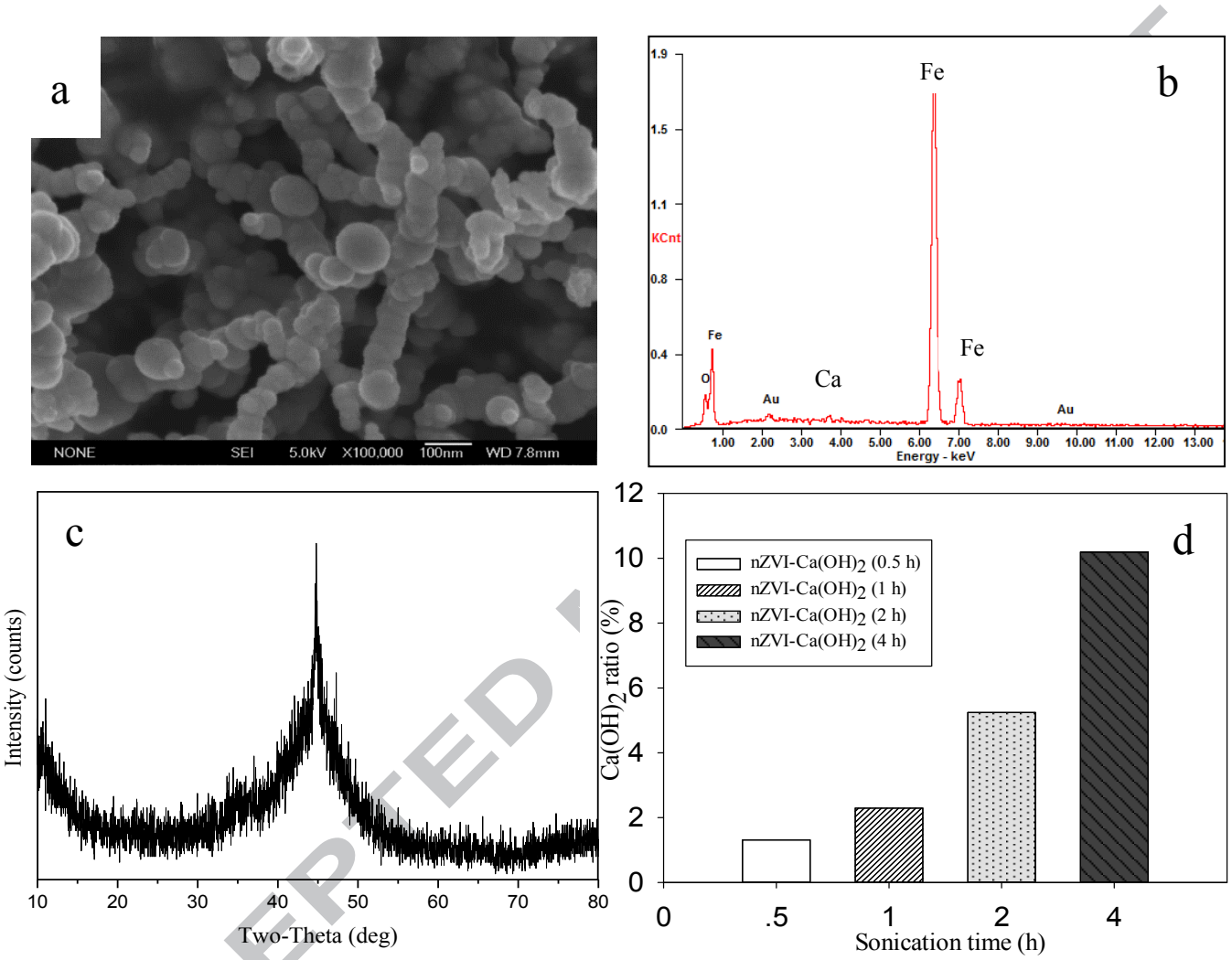

475

476 Fig. 1. (a) SEM image of nZVI-$Ca(OH)_2$ particles (sonication time: 0.5 h), (b) the

477 corresponding EDS (sonication time: 0.5 h), (c) XRD analysis of nZVI-$Ca(OH)_2$

478 particles (sonication time: 0.5 h), and (d) the content of $Ca(OH)_2$ coated on the nZVI

479 particles under different sonication time

480

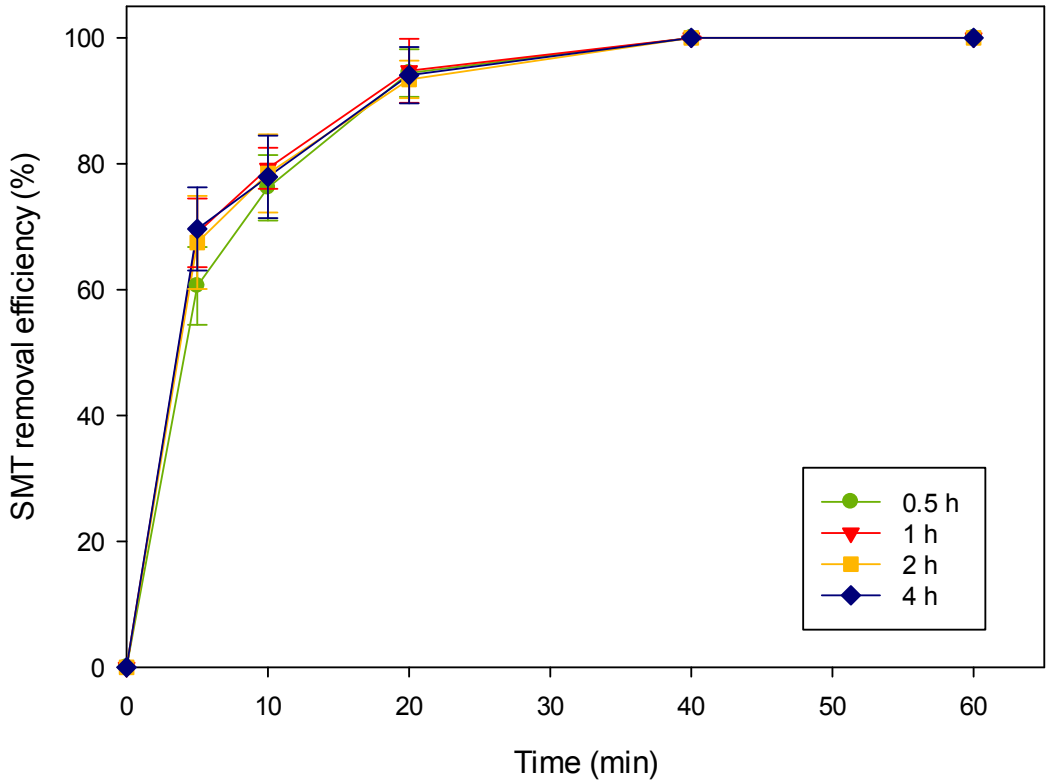

481

482 Fig. 2. Effect of sonication time during synthesis of nZVI-$Ca(OH)_2$ on SMT removal

483 by nZVI-$Ca(OH)_2$ activated PS (initial pH = 5; [SMT] = 0.025 mM; [PS] = 1 mM;

484 [nZVI-$Ca(OH)_2$] = 50 mg/L)

485

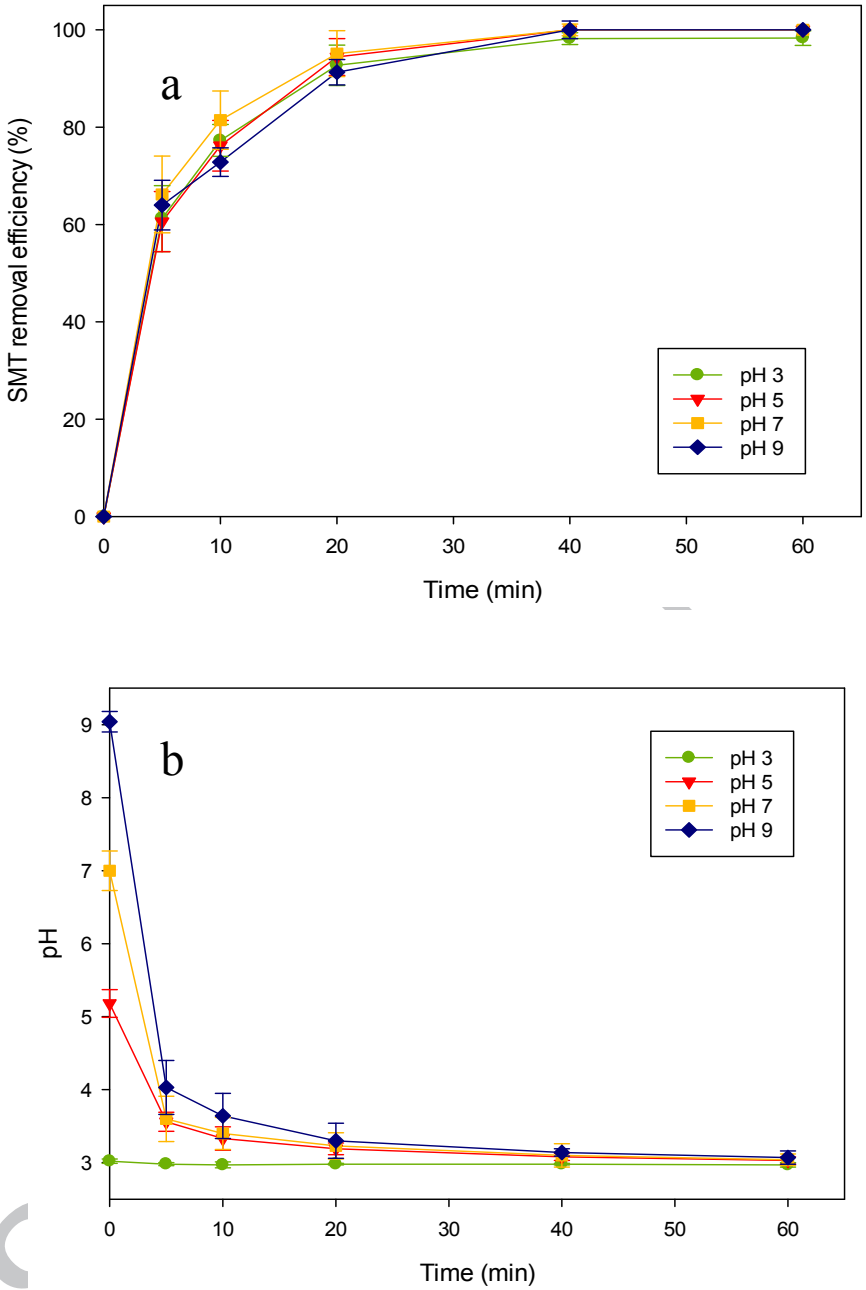

486

487

488 Fig. 3. (a) Effect of initial pH on the removal of SMT by nZVI-$Ca(OH)_2$ and (b) pH

489 changes with time ([SMT] = 0.025 mM; [PS] = 1 mM; [nZVI-$Ca(OH)_2$] = 50 mg/L)

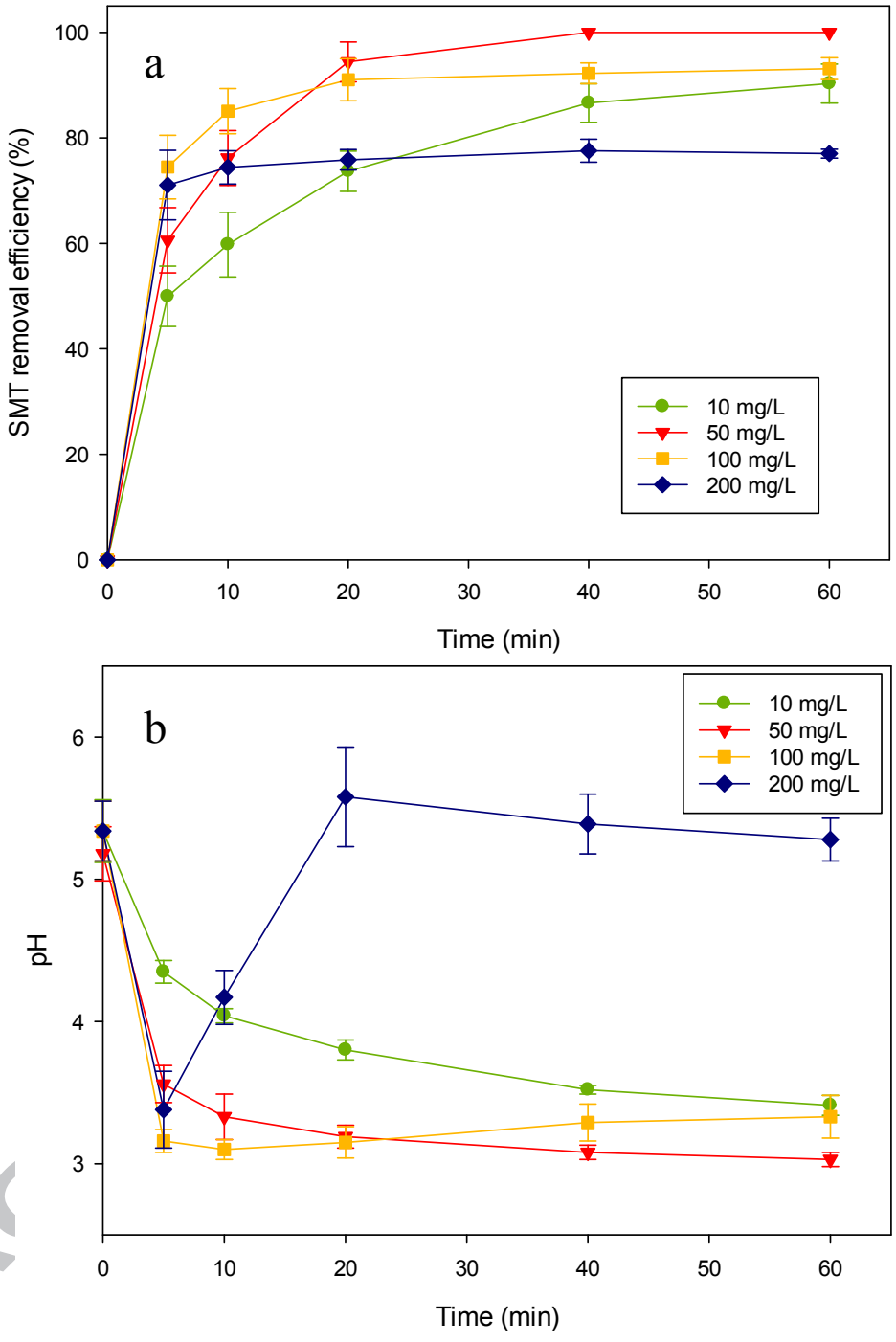

490

491 Fig. 4. (a) Effect of nZVI-Ca(OH)$_2$ dosage on the removal of SMT and (b) pH

492 changes with time in different nZVI-Ca(OH)$_2$ dosage systems (initial pH = 5; [SMT]

493 = 0.025 mM; [PS] = 1 mM)

494

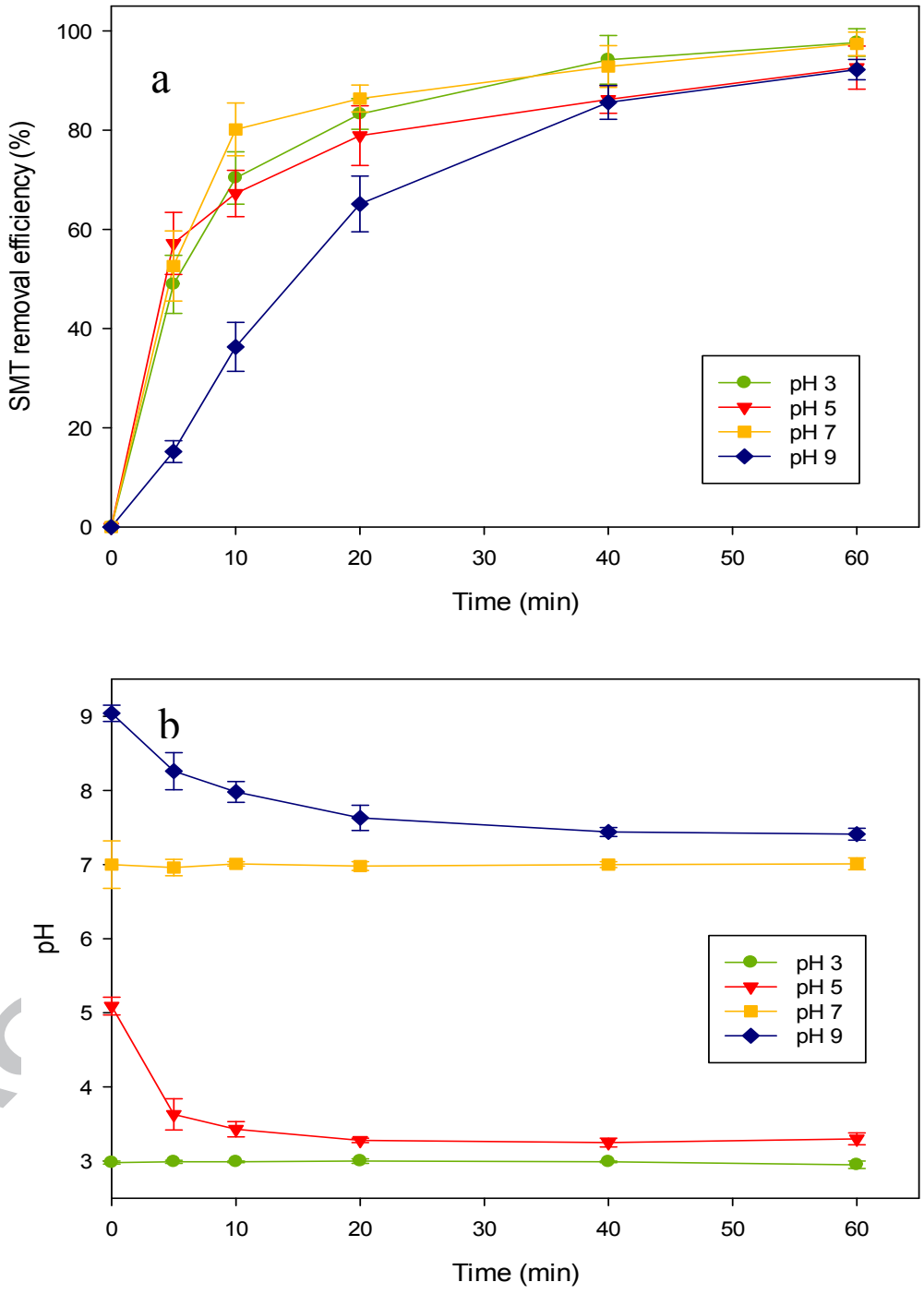

Fig. 5. (a) SMT removal by nZVI-$Ca(OH)_2$ in synthetic groundwater under different pH, and (b) pH changes with time in synthetic groundwater ([SMT] = 0.025 mM; [PS] = 1 mM; [nZVI-$Ca(OH)_2$] = 50 mg/L)

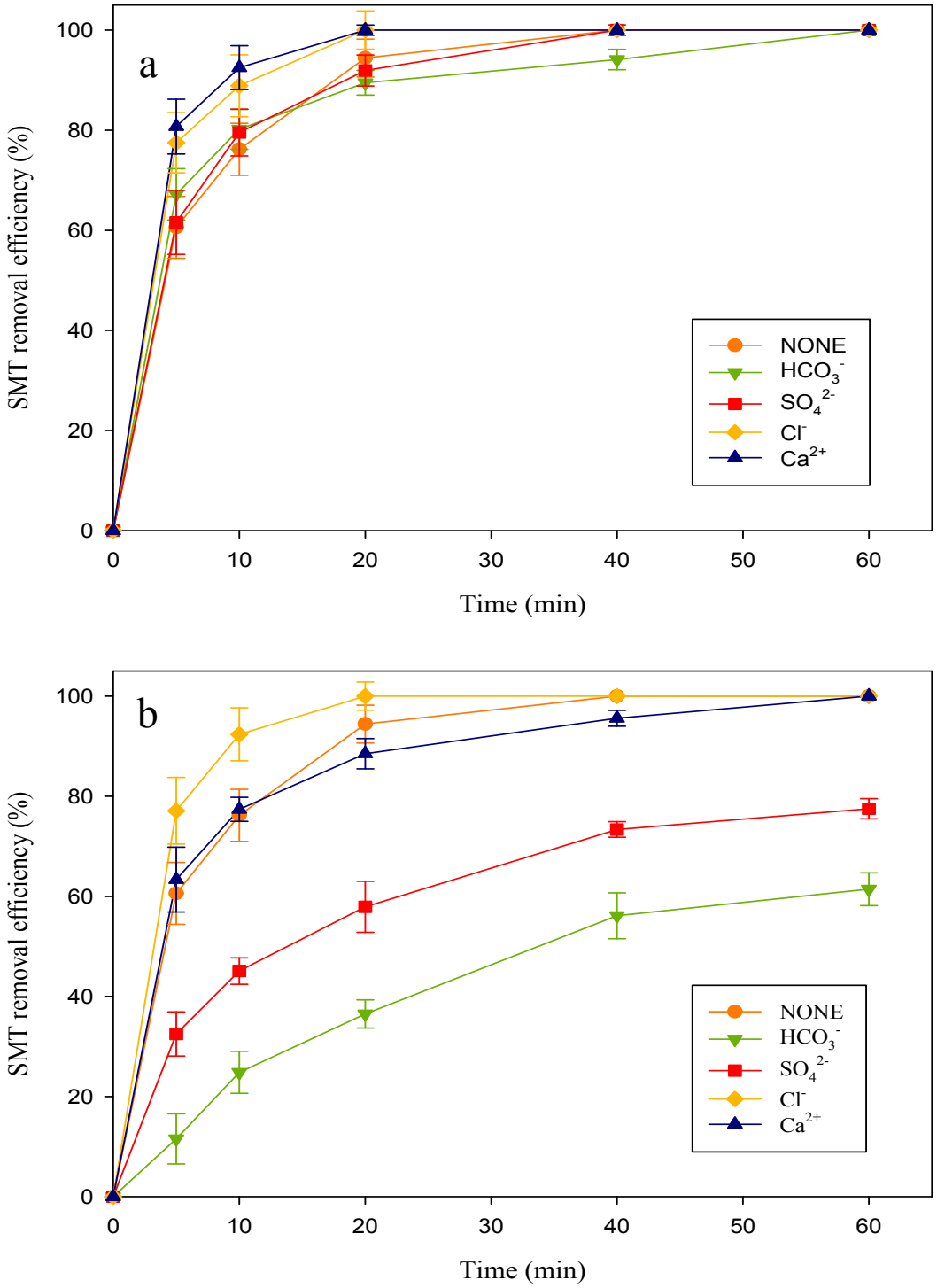

501

502 Fig. 6. Effect of typical groundwater components of different concentrations (a: 1

503 mmol/L; b: 10 mmol/L) on the removal of SMT by nZVI-$Ca(OH)_2$ activated PS

504 (initial pH = 5; [SMT] = 0.025 mM; [PS] = 1 mM; [nZVI-$Ca(OH)_2$] = 50 mg/L)

505

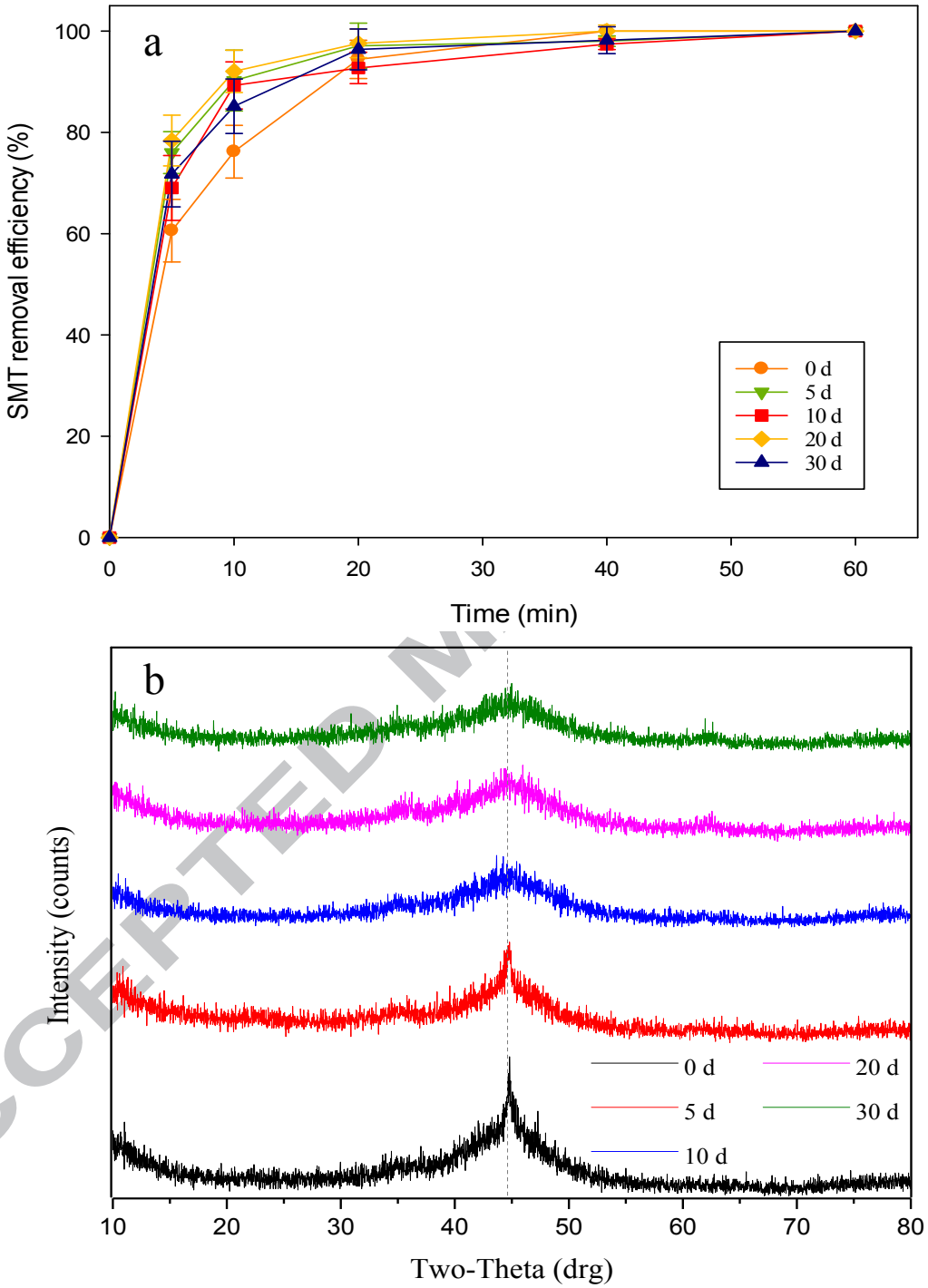

506

507 Fig. 7. (a) SMT removal by the aged nZVI-$Ca(OH)_2$ activated PS and (b) XRD

508 patterns of aged particles (initial pH = 5; [SMT] = 0.025 mM; [PS] = 1 mM; [nZVI-

509 $Ca(OH)_2$] = 50 mg/L)

- nZVI-Ca(OH)$_2$ was used as an activator of PS for the degradation of SMT
- There was an optimum dosage of nZVI-Ca(OH)$_2$ for the activation of PS to degrade SMT
- nZVI-Ca(OH)$_2$ was efficient for PS activation in synthetic groundwater at pH 3-9
- The presence of high concentration of HCO_3^- or SO_4^{2-} greatly inhibited SMT removal
- The Ca(OH)$_2$ shell can protect the inner iron core from oxidation in the air